State-dependent vulnerability of synchronization

Everton S. Medeiros,[1,2,*] Rene O. Medrano-T,[3] Iberê L. Caldas,[1] Tamás Tél,[4,5] and Ulrike Feudel[2]

[1]*Institute of Physics, University of São Paulo, Rua do Matão, Travessa R 187, 05508-090, São Paulo, Brazil*

[2]*Institute for Chemistry and Biology of the Marine Environment, Carl von Ossietzky University of Oldenburg, Carl–von–Ossietzky–Straße 9–11, Box 2503, 26111 Oldenburg, Germany*

[3]*Department of Physics, Federal University of São Paulo, Rua São Nicolau, 210, 09913-030, São Paulo, Brazil*

[4]*Institute for Theoretical Physics, Eötvös Loránd University, Pázmány Péter Sétány 1/A, H-1117 Budapest, Hungary*

[5]*MTA-ELTE Theoretical Physics Research Group, Pázmány Péter Sétány 1/A, H-1117 Budapest, Hungary*

(Received 12 April 2019; revised manuscript received 4 October 2019; published 4 November 2019)

A state-dependent vulnerability of synchronization is shown to exist in a complex network composed of numerically simulated electronic circuits. We demonstrate that disturbances to the local dynamics of network units can produce different outcomes to synchronization depending on the current state of its trajectory. We address such state dependence by systematically perturbing the synchronized system at states equally distributed along its trajectory. We find the states at which the perturbation desynchronizes the network to be complicatedly mixed with the ones that restore synchronization. Additionally, we characterize perturbation sets obtained for consecutive states by defining a safety index between them. Finally, we demonstrate that the observed vulnerability is due to the existence of an unstable chaotic set in the system's state space.

DOI: 10.1103/PhysRevE.100.052201

I. INTRODUCTION

Many complex systems, ranging from technological devices to ecology and human physiology, are composed of smaller parts operating in synchrony in order to perform their global behavior [1]. For example, in power grids, the power generators have to remain synchronized to guarantee the frequency stability of the network. Failures in this state can lead to severe power outages [2]. In ecology, phenological synchronization establishes the temporal overlap between interacting species. Such synchrony is now threatened by climate change [3]. In the heart, asynchronous pumping of the left and right ventricles leads to out-of-sync heart contractions causing severe health conditions due to low blood flow to the body [4].

In networks, the asymptotic stability of synchronous states with respect to small perturbations is well determined in the linear limit by the formalism of the *master stability function* [5,6]. Yet the impact of large perturbations has been addressed only by measurements performed in the synchronization basins, i.e., the state space configuration in the initial instant [7,8]. Additionally, the fractality of the boundaries of such synchronization basins has been also identified as a source of the sensitivity of synchronized states to perturbations [9].

However, instead of estimating whether a perturbation of an initial condition leads a network to desynchronization, one can also raise a different question. Suppose the system has already reached a completely synchronized trajectory performing some oscillatory dynamics. One now asks how vulnerable is this synchronized oscillation with respect to prescribed perturbations occurring at a certain state along the trajectory? Does it matter at which state this perturbation occurs along the trajectory? The answers to these questions are essential for the safety of technological applications as well as for designing responsible interventions in natural systems.

To address this question, we consider a random network composed of identical electronic circuits simulated numerically. By perturbing the synchronized oscillation in chronological instants of time to achieve different states, we demonstrate that the susceptibility of synchronization to disturbances changes in a nontrivial manner along the system's trajectory. A perturbation applied at one state along the trajectory could lead to a restoration of the synchronized oscillation, while the same perturbation applied in another state, very close to the previous one, could desynchronize the whole network. We call this phenomenon state-dependent vulnerability of synchronization. We analyze it by applying sets of perturbations in subsequent states along the trajectory. For these perturbation sets, we identify safe sets that still lead the network to synchronization and characterize their transformations by measuring the safety index, a measure of their alikeness. A basin stability analysis shows that the relative size of the safe sets does not change significantly between consecutive states along the trajectory, suggesting that only the location of the sets is important. Finally, we attribute the phenomenon to the existence of an unstable chaotic set in the state space and show the mechanism at which this set influences the network.

II. STATE-DEPENDENT VULNERABILITY

We study a random network composed of N electronic circuits numerically simulated via the following dimensionless

*esm@if.usp.br

dynamics [10]:

$$\begin{aligned}\dot{x}_i &= \alpha x_i + z_i + \frac{\sigma}{D_i}\sum_{j\in\mathcal{D}_i}(x_j - x_i),\\ \dot{y}_i &= z_i - f(y_i) + \frac{\sigma}{D_i}\sum_{j\in\mathcal{D}_i}(y_j - y_i),\\ \dot{z}_i &= -x_i - \beta y_i + \frac{\sigma}{D_i}\sum_{j\in\mathcal{D}_i}(z_j - z_i),\end{aligned} \tag{1}$$

where $f(y_i) = \frac{\gamma}{2}(|y_i + \gamma^{-1}| - |y_i - \gamma^{-1}|)$ describes a piecewise linear diode resistance with slope γ. The vector $\mathbf{v}_i(t) = (x_i(t), y_i(t), z_i(t))$ defines the state space of each circuit i with $i = 1, \ldots, N$. The parameters α and β are related to circuit elements. Following Ref. [10], for each circuit we fix $\alpha = 0.6$, $\beta = 2.18$, and $\gamma = 470$. The parameters σ and N are the coupling strength and the network size, respectively. The parameter D_i is the number of units to which the circuit i is connected. The set of adjacent units of i, $\mathcal{D}_i$, is specified by an adjacency matrix shown in the Supplemental Material [11]. The ordinary differential equations that simulate the electronic circuits [Eq. (1)] have been integrated by a Runge-Kutta-Fehlberg algorithm with adaptive step size. The numerically obtained trajectory is shown for points equally spaced by 0.01.

Considering first an isolated electronic circuit, i.e., $\sigma = 0$ in Eq. (1), the system exhibits a stable limit cycle $\mathbf{A}$ with dimensionless period $T = 16$, a chaotic saddle Λ embedded in the basin of attraction of $\mathbf{A}$, and an attractor at infinity. Next, we couple $N = 25$ circuits with these features in a network with coupling strength fixed at $\sigma = 0.1$. Initially, all network circuits are set to synchronize at their limit-cycle attractor $\mathbf{A}$. The synchronized state lies in a synchronization manifold $\mathbf{S}$, defined as $\mathbf{v}_1(t) = \mathbf{v}_2(t) = \cdots = \mathbf{v}_N(t)$, where all states, in the limit cycle, are generally denoted by $\mathbf{v_S}(t) = (x_S(t), y_S(t), z_S(t))$. In order to distinguish the attractor $\mathbf{A}$ of a single uncoupled circuit from the synchronized oscillating dynamics of the high-dimensional system, we refer to the latter as $\mathbf{A_S}$, the limit-cycle attractor in the $3N$-dimensional state space. However, we emphasize that in the synchronized oscillation there are no interactions between the nodes because of the vanishing coupling term. Consequently, each circuit behaves as isolated and the limit cycle $\mathbf{A}$ is a projection of $\mathbf{A_S}$ onto the state space of each circuit. Additionally, in the $3N$-dimensional state space, we refer to the chaotic set as $\mathbf{\Lambda}$, not to be confused with the chaotic saddle in the state space of a single unit denoted by Λ. The synchronized behavior of the network can be assessed by a next-neighbor error, $E_i(t) = \|\mathbf{v}_i(t) - \mathbf{v}_{i-1}(t)\|$. The perturbation applied to one unit residing on $\mathbf{A_S}$ consists of a perturbation $\mathbf{\Delta}_i = (\Delta x_i, \Delta y_i, \Delta z_i)$, directly applied to the dynamical state of a preselected circuit, i. In this manner, the dynamical state into which a perturbation brings the unit i is given by $\mathbf{v}_i(t_p) = [x_S(t_p) + \Delta x_i, y_S(t_p) + \Delta y_i, z_S(t_p) + \Delta z_i]$, the time t_p ($t_p \in [t, t + T]$) specifies all perturbed states along the trajectory starting from the state at initial instant $t = 0$ given by $\mathbf{v}_1(0) = \mathbf{v}_2(0) = \cdots = \mathbf{v}_N(0) = (-0.765, 0.003, 1.040)$.

The perturbed state $\mathbf{v}_i(t_p)$ and the one belonging to $\mathbf{A_S}$, $\mathbf{v}_S(t_p)$, at which the perturbation is applied are the central quantities in this work. In Fig. 1(a), the network is perturbed in one of the states belonging to $\mathbf{A_S}$ arbitrarily chosen to be $\mathbf{v}_S(t_{p1})$, at $t_{p1} = 4005.97$, by applying the perturbation $\mathbf{\Delta}_{19} = (0.0, 0.97, -1.14)$ also to an arbitrarily chosen unit ($i = 19$ with $D_{19} = 10$). For an alternative perturbed unit see the Supplemental Material in Ref. [11]. We observe that the system returns to the synchronization manifold $\mathbf{S}$ leading to the conclusion that the perturbed state $\mathbf{v}_{19}(t_{p1})$ belongs to the synchronization basin $\mathcal{B}$ of $\mathbf{A_S}$, i.e., $\mathbf{v}_{19}(t_{p1}) \in \mathcal{B}(\mathbf{A_S})$. As a consequence, the synchronization is restored after the perturbation and all units follow the same limit cycle $\mathbf{A}$ depicted in Fig. 1(b). Now, if the same perturbation is applied in a slightly different state specified by $t_{p1} + \Delta t$ with $\Delta t = 10^{-2}$, then we find that the network desynchronizes, indicating the opposite as before, i.e., $\mathbf{v}_{19}(t_{p1} + \Delta t) \notin \mathcal{B}(\mathbf{A_S})$, as shown in Fig. 1(c). Each unit is trapped in irregular trajectories [cf. Fig. 1(d)]. This disagreement suggests that the synchronization stability depends crucially on the particular state at which a certain perturbation is applied. Consequently, the very same perturbation imposed on the system at the same circuit may not lead the network to normal functioning in synchrony.

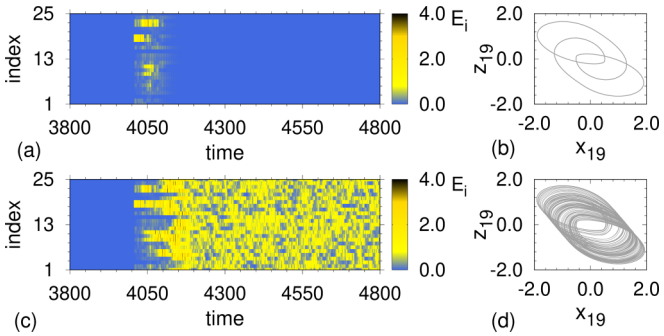

FIG. 1. Time evolution of the system. The color code indicates neighbor error, E_i. (a) The perturbation, $\mathbf{\Delta}_{19} = (0.0, 0.97, -1.14)$, is added to the local dynamics of node 19 to realize the state $\mathbf{v}_{19}(t_{p1})$ at $t_{p1} = 4005.97$. (b) Synchronized oscillation. (c) Same perturbation applied to the node 19 to realize the state $\mathbf{v}_{19}(t_{p1} + \Delta t)$ with $\Delta t = 10^{-2}$. (d) Chaotic behavior observed in the state space of node 19 in the networked system in the fully desynchronized regime.

To clarify this matter, we check the response to a particular perturbation applied at different states along the trajectory on the completely synchronized limit cycle $\mathbf{A_S}$. During one period $T = 16$ of the limit cycle $\mathbf{A_S}$, each state $\mathbf{v}_S(t_p)$ is uniquely specified by the time t_p. Hence, to study the effect of the perturbation along the system trajectory, we vary the instants of the perturbation in the interval $t_p \in [4000, 4016]$. We define an order parameter $\mathcal{Z} = (1/N)\sum_{i=1}^{N} K_i$ with $K_i = 0$ for $E_i(t_{\text{end}}) < \delta$, and $K_i = 1$ for $E_i(t_{\text{end}}) > \delta$. The overall integration time, t_{end}, is fixed at $t_{\text{end}} = 3 \times 10^4$. Employing this definition, the completely synchronized oscillation gives $\mathcal{Z} = 0$, while the completely desynchronized one gives $\mathcal{Z} = 1$. The parameter $\delta = 0.01$ controls the synchronization quality, see the Supplemental Material in Ref. [11] for this choice of δ. In Fig. 2(a), we show the component z_S of the synchronized oscillatory state as a function of the perturbation time t_p. The blue-colored (dark-gray) points indicate the z component of states in which the applied perturbation $\mathbf{\Delta}_{19} = (0.0, 0.97, -1.14)$ leads to restoration of synchronization in the network, $\mathcal{Z} = 0$. The yellow-colored (light-gray) points indicate the z component of states in which the same applied

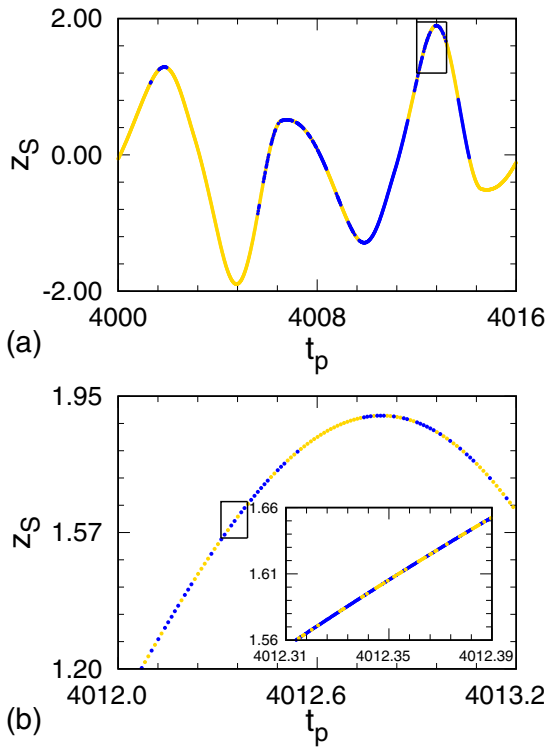

FIG. 2. (a) The z coordinate of the synchronized oscillation as function of the perturbation instant t_p. In yellow (light gray) are the z component of $\mathbf{v}_S(t_p)$ for which a perturbation, $\mathbf{\Delta}_{19} = (0.0, 0.97, -1.14)$, would desynchronize the network. The blue (dark-gray) color corresponds to z component of $\mathbf{v}_S(t_p)$ for which the perturbation restores synchronization. (b) A blow-up of the squared region of (a). The inset shows the sensitivity to the state at a finer scale.

perturbation, $\mathbf{\Delta}_{19}$, would desynchronize the network, $\mathcal{Z} = 1$. In Fig. 2(b), we highlight a very sensitive interval of the synchronized oscillation [squared region of Fig. 2(a)]. In the inset, we show a magnification of an interval in which both outcomes are mixed even at a finer scale. This confirms the observations of Fig. 1 and shows that the distribution of states leading to synchronization or desynchronization is very intricate, exhibiting a fractal-like behavior with more and more mixing of outcomes at finer and finer scales.

Next, we investigate the synchronization dynamics in the space of perturbations $\mathbf{\Delta}_i$ applied to preselected states. For the sake of visualization, we restrict ourselves to applying perturbations in the plane $\Delta x_i = 0$. In Fig. 3(a), for the perturbation leading to the state $\mathbf{v}_{19}(t_{p1})$ at $t_{p1} = 4005.97$, we show a synchronization diagram for $(\Delta z_{19} \times \Delta y_{19})$. The blue (dark-gray) color indicates perturbation regions for which the network synchronizes ($\mathcal{Z} = 0$), the safe set. The yellow color (light gray) indicates regions for which the network desynchronizes ($\mathcal{Z} = 1$). Regions in white indicate perturbations for which the solution converges to infinity, the second attractor in the system. In this figure, we find continuous regions of perturbations leading the network to both, synchronized or desynchronized, states. Additionally, we also observe regions where the perturbations leading to each behavior appear to possess a riddledlike structure [12,13]. However, to confirm this hypothesis one would need to compute, for example, the uncertainty exponent [14,15]. In Fig. 3(b), we present the synchronization diagram for a subsequent state $\mathbf{v}_S(t_{p1} + \Delta t)$ with $\Delta t = 10^{-2}$, and obtain similar characteristics for the distribution of the blue (dark-gray) points. Moreover, if the procedure is repeated for other states along the synchronized trajectory, for instance, $\mathbf{v}_S(t_{p2})$ at $t_{p2} = 4009.95$ and $\mathbf{v}_S(t_{p2} + \Delta t)$ with $\Delta t = 10^{-2}$ [Fig. 3(c) and 3(d)], we find a completely different distribution of such points, though the pictures of subsequent states along the trajectory are again similar. The white dots in the insets of Fig. 3 indicate changes, from 0 to 1, of the order parameter for subsequent states.

In order to determine the changes between perturbation planes obtained for subsequent states along the trajectory causing state-dependent vulnerability, we define a finite perturbation plane as $U = \{\Delta_{19} \in \mathbb{R}^3 \mid \Delta x_{19} = 0, \Delta y_{19} \in [-4, 4], \Delta z_{19} \in [-13, 13]\}$, as in the diagrams shown in Fig. 3. The safe set of perturbations applied at the state $\mathbf{v}_S(t_p)$ is defined as the subset of U for which $\mathcal{Z} = 0$, and denoted by $\mathcal{B}^{\mathbf{S}}_{t_p} \subset \mathcal{B}(\mathbf{A_S})$. Similarly, the unsafe set, the perturbations in U that desynchronize the network, are defined as the elements of U for which $\mathcal{Z} > 0$ and denoted by $\mathcal{B}^{\mathbf{\Lambda}}_{t_p}$. Now we estimate the fraction of the safe set $\mathcal{B}^{\mathbf{S}}_{t_p}$ that synchronizes the network after a perturbation in the state $\mathbf{v}_S(t_p)$ and also in the state $\mathbf{v}_S(t_p + \Delta t)$ by:

$$I_{t_p} = \mathrm{Vol}\big(\mathcal{B}^{\mathbf{S}}_{t_p} \cap \mathcal{B}^{\mathbf{S}}_{t_p+\Delta t}\big)/\mathrm{Vol}\big(\mathcal{B}^{\mathbf{S}}_{t_p}\big). \tag{2}$$

We call this measure the safety index, as it reflects the probability of the network to possess the same response with respect to perturbations at subsequent states along the trajectory. Hence, in Fig. 4(a), we find $I_{t_{p1}} = 0.73$, as the safety index for perturbations applied in the states $\mathbf{v}_S(t_{p1})$ and $\mathbf{v}_S(t_{p1} + \Delta t)$, and this indicates that only 73% of the perturbations in the state $\mathbf{v}_S(t_{p1})$ still synchronize the network in the state $\mathbf{v}_S(t_{p1} + \Delta t)$. The same analysis is employed for perturbations applied in the states $\mathbf{v}_S(t_{p2})$ and $\mathbf{v}_S(t_{p2} + \Delta t)$ resulting in a safety index $I_{t_{p2}} = 0.70$, Fig. 4(c). These results indicate that the safe set $\mathcal{B}^{\mathbf{S}}_{t_p}$ changes for every state along the synchronized trajectory, causing the system to be vulnerable to a prescribed perturbation in some states and resilient in others. Increasing the distance between consecutive states with a bigger time difference Δt, the safety index would decrease accordingly. Comparing the safe sets of Figs. 3(a) and 3(c), where $\Delta t = t_{p2} - t_{p1} \approx 4.0$, the dissimilarity is evident. To investigate whether the state-dependent vulnerability of synchronization is related to the relative size of the safe sets, we compute their *basin stability* [8]. To this end, for a perturbation applied to the state $\mathbf{v}_S(t_p)$, we first denote the subset of perturbations for which only finite solutions are observed as $\mathcal{Q}_{t_p} = \mathcal{B}^{\mathbf{S}}_{t_p} \cup \mathcal{B}^{\mathbf{\Lambda}}_{t_p}$, i.e., all perturbations leading to infinity are excluded. Then, for a state perturbed at t_p we estimate the measure $S_{t_p} = \mathrm{Vol}(\mathcal{B}^{\mathbf{S}}_{t_p})/\mathrm{Vol}(\mathcal{Q}_{t_p})$ that constitutes an estimate of the volume of $\mathcal{Q}_{tp}$ occupied by the safe set $\mathcal{B}^{\mathbf{S}}_{t_p}$. For the synchronization diagrams, we obtain $S_{tp1} = S_{tp1+\Delta t} = 0.213$ [Fig. 4(b)] and $S_{tp2} = 0.161$ and $S_{tp2+\Delta t} = 0.164$ [Fig. 4(d)]. These findings demonstrate that the relative volume of the safe sets does not change significantly for subsequent states

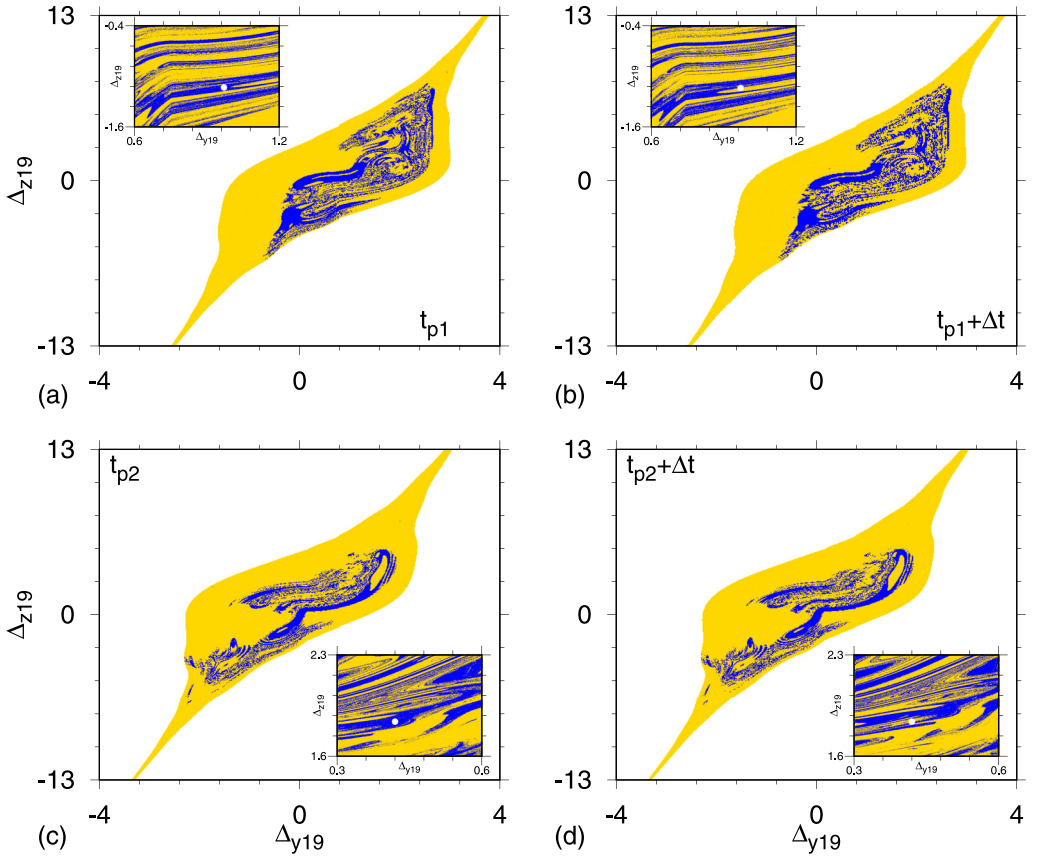

FIG. 3. [(a) and (b)] Synchronization diagrams, $\Delta z_{19} \times \Delta y_{19}$, obtained by perturbing the state $\mathbf{v}_S(t_{p1})$ at $t_{p1} = 4005.97$ and $\mathbf{v}_S(t_{p1} + \Delta t)$ with $\Delta t = 10^{-2}$, respectively. The color encodes the order parameter, blue (dark gray) for $\mathcal{Z} = 0$ (synchronized) and yellow (light gray) for $\mathcal{Z} = 1$ (completely desynchronized). [(c) and (d)] Synchronization diagrams for two different consecutive states $\mathbf{v}_S(t_{p2})$ at $t_{p2} = 4009.95$ and $\mathbf{v}_S(t_{p2} + \Delta t)$ with $\Delta t = 10^{-2}$, respectively. The white dots in the insets indicate changes of $\mathcal{Z}$.

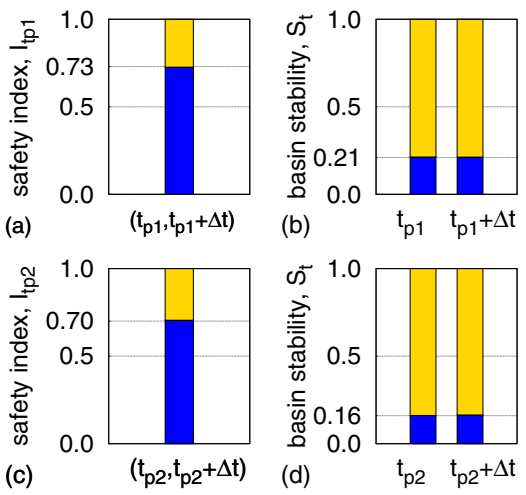

FIG. 4. In (a) the blue (dark-gray) color indicates the safety index between synchronization diagrams obtained for two consecutive states $\mathbf{v}_S(t_{p1})$ at $t_{p1} = 4005.97$ and $\mathbf{v}_S(t_{p1} + \Delta t)$ with $\Delta t = 10^{-2}$. (b) The blue (dark-gray) color indicates the corresponding basin stability of the syncronization diagrams analyzed in (a). In (c), the blue (dark-gray) color indicates the safety index for two different consecutive states $\mathbf{v}_S(t_{p2})$ at $t_{p2} = 4009.95$ and $\mathbf{v}_S(t_{p2} + \Delta t)$ with $\Delta t = 10^{-2}$. (d) The blue color (dark gray) indicates the corresponding basin stability of the synchronization diagrams analyzed in (a).

along the synchronized trajectory, i.e., $S_{t_p} \approx S_{t_p+\Delta t}$. Therefore, the state-dependent vulnerability of synchronization is only related to changes in the location of $\mathcal{B}^{\mathbf{S}}_{t_p}$ with respect to each point on the limit cycle $\mathbf{A_S}$ and not to the relative size of the safe sets. As a consequence, the safety index is a suitable indicator of this kind of vulnerability, while basin stability is not a sensitive measure. The safety index reflects how synchronization diagrams change from one state to another; therefore, it measures how many perturbations identified as safe at one state can turn into unsafe ones at a subsequent state. By contrast, basin stability measures the relative size of the safe set. This relative size remains almost unchanged for subsequent states along the trajectory, while its location in state space changes substantially indicated by the safety index. The relative size of the safe sets measured by basin stability varies only over larger time intervals within the period T, e.g., comparing them at the time instants t_{p1} and t_{p2}. Basin stability is thus not an appropriate measure for state-dependent vulnerability with respect to perturbation applied along one cycle of the synchronized trajectory.

III. THE MECHANISM OF STATE-DEPENDENT VULNERABILITY

The mechanism behind this phenomenon is related to the chaotic set $\mathbf{\Lambda}$ lying very close to the stable limit cycle $\mathbf{A_S}$.

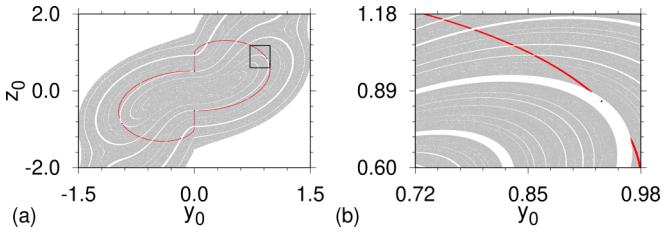

FIG. 5. (a) Basin of attraction of the limit cycle **A** on the plane $x_0 = 0$ of the uncoupled circuit, i.e., $\sigma = 0$ in Eq. (1). The six blue (dark-gray) dots represent the intersections of **A** with this section, while red (black) dots mark the projection of the chaotic saddle Λ. Gray dots mark the initial conditions having lifetime longer than 50 and provide an approximation to the stable manifold of Λ. (b) A magnification of the black ractangle in (a) showing the detail of the chaotic saddle. Note how close the saddle Λ is located to **A**.

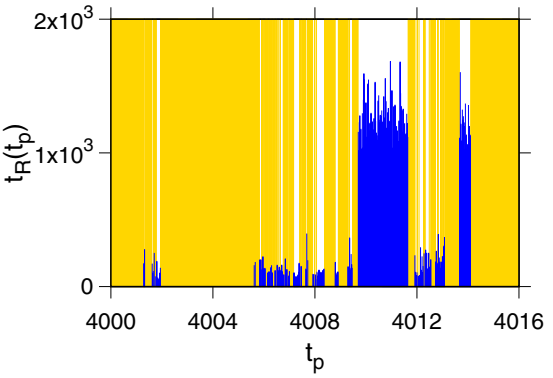

FIG. 6. Time for the synchronized state be restored, t_R, as function of the perturbation instants, t_p. The perturbation is given by $\mathbf{\Delta}_{19} = (0.0, 0.97, -1.14)$. The yellow (light-gray) bars delimitate perturbation instants for which the system desynchronizes, while the height of the blue (dark-gray) bars represents the restoring time of synchronization.

The low values of the basin stability shown in Figs. 4(b) and 4(d), i.e., the large fractions of unsafe perturbations, indicate that a large portion of the system's state space is covered by the stable manifold of the chaotic saddle **Λ**. This high-dimensional chaotic set appears from the individual ones, occurring in every single circuit. Considering a Poincaré section at $x = 0$ for an individual uncoupled circuit, i.e., $\sigma = 0$ in Eq. (1), we show in Fig. 5 a projection of the chaotic saddle Λ in red (black) obtained by the sprinkler method [16] and an approximation of its stable manifold (gray dots). This approximation is obtained by computing the saddle's escape time defined as the number of crossings in the Poincare section before a disk of radius $\varepsilon = 10^{-4}$ around the attractor points is reached. The statistics of such escape times obeys an exponential distribution [16,17]. However, coupling all those circuits, another large chaotic set **Λ** emerges being difficult to obtain [18]. As demonstrated in Ref. [9], this chaotic set appears to be an attractor for the coupled system or, at least, a chaotic saddle with extremely long transients with escape times beyond our numerical computations. Hence, when the system is coupled, there is a competition, in each unit, between the network coupling and the chaotic dynamics in the vicinity of the chaotic set **Λ**. If the coupling is not strong enough to attract the perturbed unit quickly back to the synchronization manifold, despite the perturbed unit, additional ones are pulled to the chaotic set. Once a critical number of units approach this chaotic set, escaping from it becomes very unlikely [19,20], trapping the high-dimensional system in a chaotic desynchronized behavior for times indefinitely long. This mechanism is explained in detail in Ref. [9] for perturbations applied in the initial instant of time. Here we show a much stronger consequence of such a phenomenon, the outcome of such a competition between the coupling strength and the chaotic dynamics leading to synchronization or desynchronization, exhibits an intricate dependence on the current state of the system along its oscillatory trajectory.

Furthermore, we remark that the state-dependent vulnerability of synchronization in the example considered in this study is along a limit cycle. It means that the profile of vulnerability is repeated every period T of this cycle. Therefore, the reported phenomenon in this particular case can be interpreted as a phase-dependent phenomenon similar to others observed in low-dimensional systems, such as phase-dependent noise-induced switching between different limit cycles in a phytoplankton-zooplankton model [21] and phase-sensitive excitability [22].

Now, in order to demonstrate the state dependence of the phenomenon, we analyze the trajectory of the perturbed unit for perturbations, $\mathbf{\Delta}_{19} = (0.0, 0.97, -1.14)$, applied at different states of the synchronized trajectory. Since in one cycle of the oscillation, $t_p \in [4000,4016]$, each trajectory's state is uniquely expressed by the time t_p, we show this analysis as a function of the perturbation instants as in Fig. 2. Hence, for the states in which the synchronization manifold is restored, the system can be examined by computing the transient time to return to the synchronized oscillation [23]. Here, the transient time t_R is defined as the time needed for the order parameter $\mathcal{Z}$ go to zero, i.e., $E_i(t) = \|\mathbf{v}_i(t) - \mathbf{v}_{i-1}(t)\| < 0.01 \ \forall \ i$. In Fig. 6, we show the return time t_R, needed to restore complete synchronization as a function of the perturbation instants t_p which is equivalent to the phase of the limit cycle. The yellow (light-gray) bars correspond to perturbations instants for which full desynchronization occurs, i.e., $t_R \to \infty$. The height of the blue (dark-gray) bars indicates the finite return time for perturbations applied at their respective instant of time. The variability found in the finite values of t_R and the nontrivial distribution of the yellow (light-gray) bars indicates the sensitivity encountered by the perturbed unit depending on the perturbation instants and, consequently, on the state along one oscillation cycle.

IV. CONCLUSIONS

We report the existence of an intricate state dependence of the vulnerability of the synchronized oscillations in a network composed of identical electronic circuits numerically simulated. By perturbing the synchronized dynamics in consecutive states along the trajectory, we find that synchronization breaks down for some states while it persists for others. Additionally, the states at which perturbations lead to synchronization or desynchronization, respectively, form a fractallike

set along the synchronized trajectory. This implies that next to a safe state there can be an unsafe one and vice versa.

The state-dependent vulnerability of synchronization is the result of the interplay between the network coupling and the dynamics on the chaotic saddle. It is important to note that the amplitudes of the perturbations involved exceed the range of the validity of linear stability of synchronized states. Therefore, our description relies on numerical analysis, as analytical approaches are hardly possible. Another obstruction to analytical approaches is the difficulty to analytically compute chaotic saddles even for the simplest nonlinear maps. Possible extensions of this analysis could be based on further numerical studies computing the distance between the saddle and the periodic orbit [24] or the high-dimensional saddles themselves for smaller networks of simpler dynamical systems computed by the stagger-and-step method [18].

The mechanism behind this intriguing phenomenon of state-dependent vulnerability is the existence of a chaotic set close to the synchronized trajectory. We point out that such sets related to transient chaos are a rather common phenomenon characteristic for several classes of dynamical systems. These classes are (1) systems possessing period-doubling cascades leading to chaos with embedded periodic windows, found in many physical applications like mechanical oscillators, laser systems, or electronic circuits; (2) systems possessing period-adding cascades like in many excitable systems important to neuroscience; and (3) systems possessing a high degree of multistability, i.e., a multitude of coexisting attractors possessing fractal basin boundaries, like most systems with weak damping. As a consequence, the reported phenomenon plays an important role whenever dynamical systems of the classes mentioned above are coupled and their synchronization behavior is studied. Moreover, we would like to emphasize that this phenomenon does occur not only in model systems described by ordinary differential equations but also in discrete-time systems. We observe state-dependent vulnerability in networks of different nonlinear maps, e.g., logistic and Hénon maps. These results are to be published elsewhere. Additionally, we remark that, besides the synchronization in a periodic orbit discussed here, the same phenomenon occurs for systems synchronized in a chaotic attractor. Therefore, the state-dependent vulnerability of synchronization is a very ubiquitous phenomenon.

Furthermore, the implications of the state-dependent vulnerability of synchronization are twofold: On the one hand, it is a warning that a harmless perturbation applied to a complex network in its past can have different consequences if applied in a different instants along the synchronized trajectory. On the other hand, the knowledge about the possibility to destroy synchronization when particular perturbations are applied in the right state can be a useful tool in such cases when synchronization is undesired. Hence, state-dependent vulnerability offers to determine those attractor regions in which interventions aiming at the break of synchrony can be successful. For instance, a hypersynchronous state in the brain must be suppressed to terminate an epileptic seizure [25,26]. Additionally, in ecology, the occurrences of synchronization among different patches are associated with an increasing risk of global extinction of the species in the ecosystem [27,28]. The knowledge of states in which synchronization is vulnerable may now increase the likelihood of successful development of conservation strategies for saving such ecosystems from extinction.

ACKNOWLEDGMENTS

This work was supported by FAPESP (Processes No. 2018/03211-6, No. 2013/26598-0, No. 2015/50122-0, and No. 2017/05521-0) and the National Research, Development and Innovation Office of Hungary under Grant No. K-125171.

[1] A. Pikovsky, M. Rosenblum, and J. Kurths, *Synchronization: A Universal Concept in Nonlinear Sciences* (Cambridge University Press, Cambridge, UK, 2003).
[2] A. E. Motter, S. A. Myers, M. Anghel, and T. Nishikawa, Nat. Phys. **9**, 191 (2013).
[3] W. W. Deacy, J. B. Armstrong, W. B. Leacock, C. T. Robbins, D. D. Gustine, E. J. Ward, J. A. Erlenbach, and J. A. Stanford, Proc. Natl. Acad. Sci. USA **114**, 10432 (2017).
[4] R. A. Gray, A. M. Pertsov, and J. Jalife, Nature (London) **392**, 75 (1998).
[5] L. M. Pecora and T. L. Carroll, Phys. Rev. Lett. **80**, 2109 (1998).
[6] L. M. Pecora, T. L. Carrol, G. Johnson, D. Mar, and K. S. Fink, Int. J. Bif. Chaos **10**, 273 (2000).
[7] D. A. Wiley, S. H. Strogatz, and M. Girvan, Chaos **16**, 015103 (2006).
[8] P. J. Menck, J. Heitzig, N. Marwan, and J. Kurths, Nat. Phys. **9**, 89 (2013).
[9] E. S. Medeiros, R. O. Medrano-T, I. L. Caldas, and U. Feudel, Phys. Rev. E **98**, 030201(R) (2018).
[10] R. Stoop, P. Benner, and Y. Uwate, Phys. Rev. Lett. **105**, 074102 (2010).
[11] See Supplemental Material at http://link.aps.org/supplemental/10.1103/PhysRevE.100.052201 for the adjacency matrix, for an alternative perturbed unit and for the choice of the synchronization quality.
[12] J. Alexander, J. A. Yorke, Z. You, and I. Kan, Int. J. Bif. Chaos **02**, 795 (1992).
[13] M. Woltering and M. Markus, Phys. Rev. Lett. **84**, 630 (2000).
[14] C. Grebogi, S. W. McDonald, E. Ott, and J. A. Yorke, Phys. Lett. A **99**, 415 (1983).
[15] S. W. McDonald, C. Grebogi, E. Ott, and J. A. Yorke, Physica D **17**, 125 (1985).
[16] Y.-C. Lai and T. Tél, *Transient Chaos* (Springer-Verlag, New York, 2011).
[17] T. Lilienkamp, J. Christoph, and U. Parlitz, Phys. Rev. Lett. **119**, 054101 (2017).
[18] D. Sweet, H. E. Nusse, and J. A. Yorke, Phys. Rev. Lett. **86**, 2261 (2001).
[19] J. P. Crutchfield and K. Kaneko, Phys. Rev. Lett. **60**, 2715 (1988).
[20] Y.-C. Lai and R. L. Winslow, Phys. Rev. Lett. **74**, 5208 (1995).
[21] J. A. Freund, S. Mieruch, B. Scholze, K. Wiltshire, and U. Feudel, Ecol. Complex. **3**, 129 (2006).
[22] I. Franović, O. E. Omel'chenko, and M. Wolfrum, Chaos **28**, 071105 (2018).

[23] T. Lilienkamp and U. Parlitz, Phys. Rev. Lett. **120**, 094101 (2018).
[24] M. Joglekar, U. Feudel, and J. A. Yorke, Phys. Rev. E **91**, 052903 (2015).
[25] K. Lehnertz and C. E. Elger, Phys. Rev. Lett. **80**, 5019 (1998).
[26] P. Jiruska, M. de Curtis, J. G. R. Jefferys, C. A. Schevon, S. J. Schiff, and K. Schindler, J. Physiol. **591**, 787 (2013).
[27] J. C. Allen, W. M. Schaffer, and D. Rosko, Nature (London) **364**, 229 (1993).
[28] M. Heino, V. Kaitala, E. Ranta, and J. Lindström, Proc. R. Soc. Lond. Ser. B: Biol. Sci. **264**, 481 (1997).